*International Journal of Scientific Research and Modern Education (IJSRME)*
*ISSN (Online): 2455 – 5630*
*(www.rdmodernresearch.com) Volume I, Issue II, 2016*

# CHARACTERISATION OF Cr DOPED CuO NANOPARTICLES AND ITS PERFORMANCE IN SOLAR CELL

**K. V. Jayasree*, Dr. Neelakandeswari** &**
**D. V. Ezhilarasi Gnana Kumari*****

* Associate Professor, Department of Physics, NGM College, Pollachi, Coimbatore, Tamilnadu
** Department of Nano Technology, Sri Ramakrishna Engineering College, Vattamalaipalayam, Coimbatore, Tamilnadu
*** Department of Physics, NGM College, Pollachi, Coimbatore, Tamilnadu

**Abstract:**

*Pure and $Cr^{2+}$doped Copper oxide (CuO) nanoparticles were synthesized by simple precipitation method and subjected to photovoltaic activity by forming nanopowder –thin film as light absorbing layer on an indigenously fabricated heterojunction by Doctor-Blade method. Effect of concentration of the dopant (2, 4, and 6 mol%) on the properties of CuO was analyzed from X-Ray Diffraction pattern (XRD), Scanning Electron Microscopy(SEM) Energy Dispersive Analysis (EDAX), UV-Vis studies and Photoluminescence spectroscopy (PL) . The XRD result clearly indicates that the samples are polycrystalline in nature and belongs to monoclinic crystal structure. It was revealed that due to the addition of dopants the average grain size varies from 22.14nm – 17.5nm.The improvement in the band gap from 2 to 2.5e V is elucidated from the optical analysis. The results showed that the $Cr^{2+}$ dopant did not give rise to any new PL signal, but it could improve the intensity of PL spectra, which was possibly attributed to the increase in the content of surface oxygen vacancies and defects after doping $Cr^{2+}$. Solar cell parameters were measured using Autolab potentiostate coupled with Metro solar simulator and explored that the cell parameter for 4mol% doping projected a comparatively better results for power conversion efficiency.*

**Introduction:**

Transition metal oxide (MOs) semiconductors are one of the most significant class of nanostructure semiconductors owing to their wide and tuneable band gap and it is cost effective, ease fabrication and non hazardous in nature. The higher surface to volume ratio and its quantum size effect are largely exploited for the fabrication of gas sensors, electronic and optoelectronic devices especially solar cell. Metal oxide nanoparticles are gaining attention as new materials in the applications of photovoltaic activity [1-4]. Among these CuO is chosen because of its unique properties such as narrow band gap, non –toxicity, and abundancy. Attempts were made to use CuO nanoparticles as light absorbing material in solar cell technology [5]. Ranjan bar et al reports CuO have been spin coated at 100nm thick on FTO substrate and produce a power efficiency 'ŋ' of 1.5 X $10^{-4}$ ,Fill Factor 0.25, $J_{SC}$ of 13 $\mu Acm^{-2}$ ,Voc of 45mV and concluded that the formation of higher quality CuO may improve future cell efficiency [6]. Yusheng Xia reports that the fabrication of CuO nanoleaves on a Si wafer which shows an optical absorption increase and reduction in reflection in the 250 -1250nm. The CuO- Si junction produces a bulk potential result in a photo generated electron and holes increasing the carrier lifetime. The power conversion efficiency has been reported to increase by 17.90% and the current efficiency to 10.30% [7]. Peng et al reports a growth of p- CuO nanowires array with simple thermal oxidation and fabrication of p-CuO and n-ZnO layer heterojunction which exhibits a photocurrent of 0.264μm with overall efficiency of 0.1% [8].

Meanwhile very few reports are available on photoelectric conversion properties of CuO doped with Chromium in literature. Obulapathi et al reports that the Chromium doping in CuO has enhanced the transmittance and optical band gap [9]. Buvenesware et el reports the doping of Cr in CuO has enhanced the ammonia sensing at room temperature due to higher surface area [10] P. Gwizdz et al reports Cr doping in $TiO_2$ gas sensor has different sensing properties as a result of $Cr^{2+}$ doping a change of conductivity from n type to p type was also observed in 1 atomic wt % doping [11].

In this paper we present our results on the modulation of structural morphological and optical properties of chromium doped cupric oxide nanostructures synthesised by Co-precipitation method. The utilization of prepared pure CuO nano structures and Cr doped CuO nanostructures for light absorption of solar spectrum is mainly focused.

**Materials and Methods:**

**Materials:**

The chemicals used in this study were all analytical grade and used without any further purification. Copper nitrate or Cupric nitrate [$Cu(No_2)_2.3H_2o$], glacial acetic acid[$CH_3COOH$], chromium nitrate{$Cr(H_2O)_6](No_3)_3.3H_2o$} ,ethanol, and sodium hydroxide [NaOH] were the chemicals used in the reaction process. Muffle furnace and magnetic stirrer were required to complete the experiment.

**Characterisation of Nanostructures:**

The structural analysis was performed by powder X ray diffraction (XRD X Pert PRO PW -1830 Philps Germony) .The vibrational functional group was recorded using Fourier Transform Infrared spectroscopy(FTIR spectrum 100 Perkin Elmer). The microscopical analysis of the samples was carried out by a scanning electron microscope (SEM JSM-200 JEOL USA) equipped with energy dispersive spectroscopy (EDS). The optical properties were determined by recording the absorption spectra using UV Spectra photometer (Lamda 20 Perkinelmer). Photoluminescence spectrophotometry was measured on a Perkin –Elmer LS 55 spectrophotometer. The fabricated solar cell heterojuctions were then tested using a solar simulator (Autolab potentiostate coupled with Metro solar cell)

**Synthesis of Nanostructures:**

Pure and Cr doped CuO nanostructures were prepared by co-precipitation method. For the synthesis of pure CuO nanostructure, copper nitrate ($Cu (NO_2)_2.3H_2O$) was dissolved in doubly deionised water to which 1 ml Glacial acidic acid was added. The obtained aqueous solution was stirred in magnetic stirrer till it reaches the temperature of 100˚C. An aqueous solution of sodium hydroxide (NaOH) was added drop-wise under continuous stirring until it becomes a black precipitate. The precipitate thus obtained was filtered out and washed with distilled water and ethanol several times alternatively to remove any impurities present. It was further centrifuged and dried at 70˚C for 30 minute. This product was sintered to 400˚C for one hour to get better crystalline copper oxide nanopowder. For Cr doped CuO, appropriate amount of copper Nitrate ($Cu (NO_2)_2.3H_2O$) and chromium nitrate ($CrNO3. 6H_2O$,) were dissolved in doubly deionized water to get 2, 4 and 6 mol% Cr doped CuO nanostructures following the same procedure.

**Solar Cell Fabrication:**

The photovoltaic ability of the synthesized pure and Cr doped CuO nanostructures was examined in an indigenously designed photovoltaic heterojunction set up and the experimental procedures were maintained similar to that reported already [12]

Scotch tape was applied on four corners of the conducting side of ITO glass; the scotch tape thickness is measured by using electronic digital calliper. The $TiO_2$ paste was smeared with a razor blade on one side of the ITO glass. Now ITO glass plate was annealed keeping on top of a hot plate to 450 ºC for 30 minutes. After 30 minutes, the ITO glass was left to cool till room temperature. On this, $TiO_2$ paste was smeared and annealed again to the temperature for about 30 minutes. The prepared CuO: Cr(Cr=0%,2%,4% and 6%) samples were mixed with Triton X-100 to make it into a paste and this paste was spread on $TiO_2$ and again heated to 450 ºC for 30 minutes. This was cooled to room temperature and finally a Copper plate of thickness 1mm was used to make an electrical contact. Poly Iodine electrolyte (0.1M $I_2$ and 0.2 M KI) was prepared as per literature and filled between CuO layer and Cu plate and then sealed. Both the electrode and counter electrode were combined facing each other by a binder clips. Using binder clip, the solar cell was sandwiched together. The steps of procedures used are shown in Fig-1[13].


Figure 1: Steps of fabrication of heterojunction using Dr. Blade method

**Result and Discussion:**

**Structural Analysis:**

The crystallite size and the crystalline structure of the prepared samples were characterized by X-Ray diffractogram**.** Figure 2 represents XRD plot for pure CuO and Chromium doped CuO nanostructures at room temperature .The curves a,b,c,d represents the pure CuO and Cr- doped CuO to 2 mol %,4 mol % and 6 mol % respectively .From XRD diffractogram it is inferred that the particles are polycrystalline innature and their 2θ values of the prominent peaks are 35.01º, 39.81º and 49.14º, corresponds to reflections from (-1,1,1), (1,1,1) and (2,0,2) of (h,k,l) value with reference to JCPDS card no. 89-5895.It is notable that all the samples are monoclinic in structure .The absence of impurity peaks corresponding to $Cu_2O$ and Cu (OH) indicates the single phase formation of CuO nanoparticles. A small shift in 2θ to the higher angles is projected as the dopant rate increased. Referring to b-d in the Fig-2 the intensity of the peak reduces for all the doped samples as the concentration increased to 2 mol %, 4mol % and 6mol% respectively.

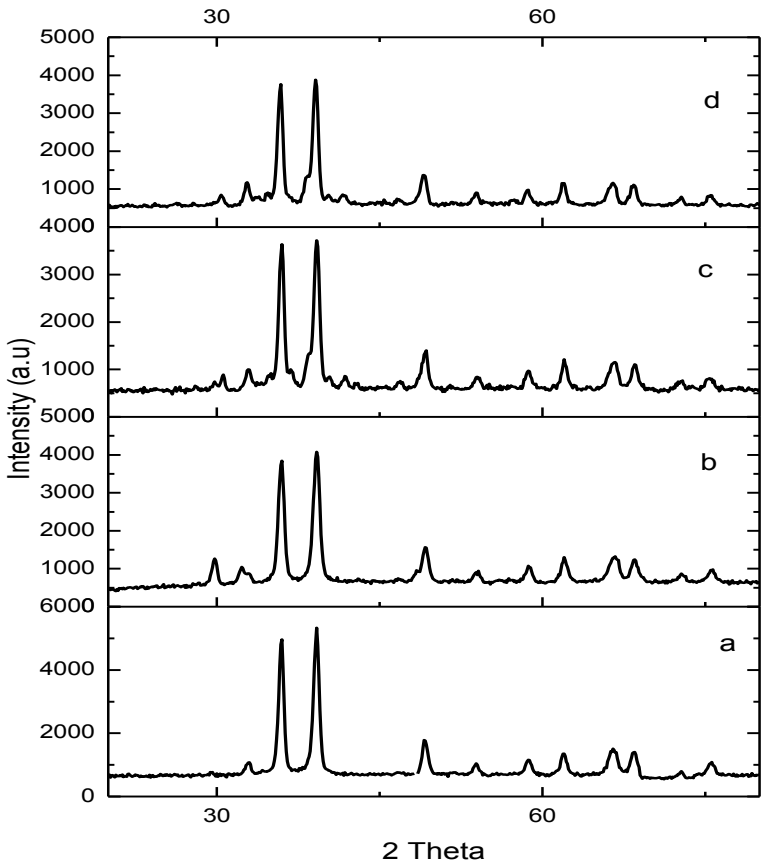


Figure 2: XRD Diffractrogram of CuO and Cr doped CuO samples

Calculated crystallite size, Lattice parameter and microstrain of the prepared samples were given in Table 1, which revealed that, as the concentration of dopant increases, particles size decreases, this may be due to replacement of $Cu^{2+}$ ions by $Cr^{4+}$ ions. [14]

Table 1: Lattice Parameters

| Sample | Crystallite Size nm | Lattice parameter | | | Microstrain |
|---|---|---|---|---|---|
| | | A | b | C | |
| CuO | 22.69 | 4.662 | 3.449 | 5.065 | 0.15 |
| CuO+ 2% | 19.42 | 4.660 | 3.445 | 5.065 | 0.18 |
| CuO+4% | 21.13 | 4.659 | 3.443 | 5.063 | 0.16 |
| CuO+6% | 21.85 | 4.671 | 3.451 | 5.127 | 0.15 |

The ionic radius of $Cr^{4+}$ (0.44) is smaller than that of $Cu^{2+}$ (0.73) leads to reduction in the crystallite size.[15] The shift in the peak position compared to pure indicates a slight distortion in the symmetry of the system due to the creation of defects and vacancies in the system. This is attributed to the charge imbalance created from Cr doping in Cu lattice [16] .The decrease in the peak intensity confirms increase in the electron density indicating loss of crystalinity owing to lattice distortion [17].

**Morphological Analysis:**

The SEM micrographs of pure and (2, 4 and 6 mol %) Cr doped CuO samples are shown in Fig-3 (a,b,c,d). The SEM micrograph of pure CuO sample Fig.3(a) shows a uniform formation of CuO phase of spherical particles with particle size 50-60nm.It is noted that for 2mol% Cr doped nanostructures it gets agglomerated and changes to thin varying plates for 4mol% and thick rods for 6mol%. The average particle size for 2

mol % and 4 mol % are found to be 70nm and 80nm. The presence of Cr in doped samples is confirmed from the EDAX analysis. EDAX spectra of pure and doped CuO nanoparticles are shown in Fig.3. It is clear from Fig. (b), (c) and (d) that Cr is successfully incorporated into the CuO system. The atomic and weight percentage of the samples are tabulated in Table-2.

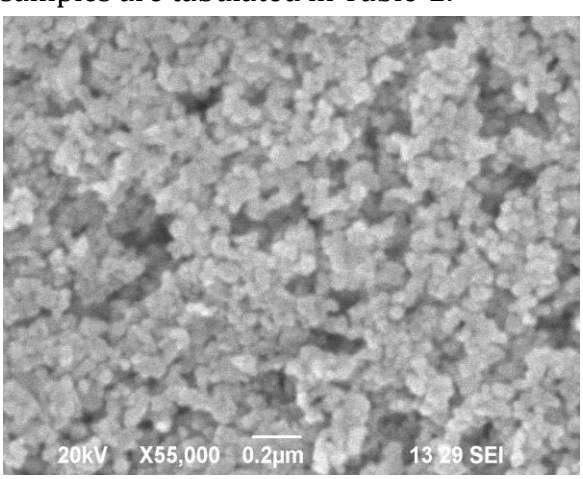


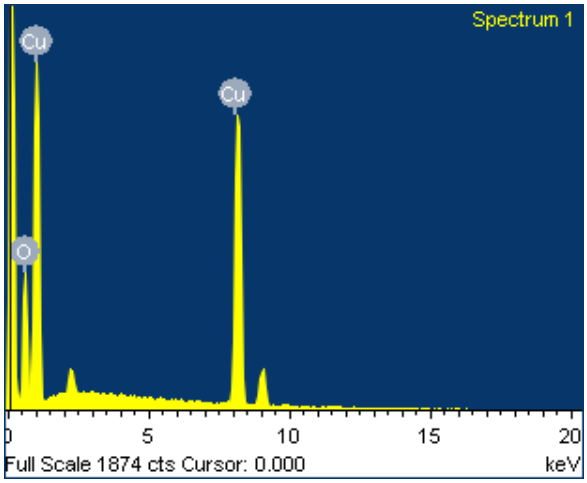


(a) SEM Micrograph and EDAX Spectra of Pure CuO

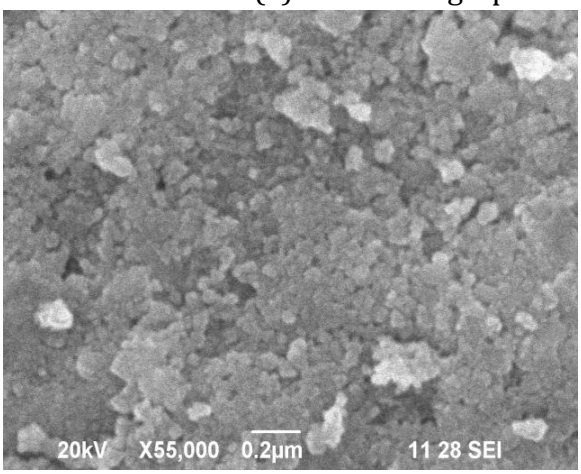


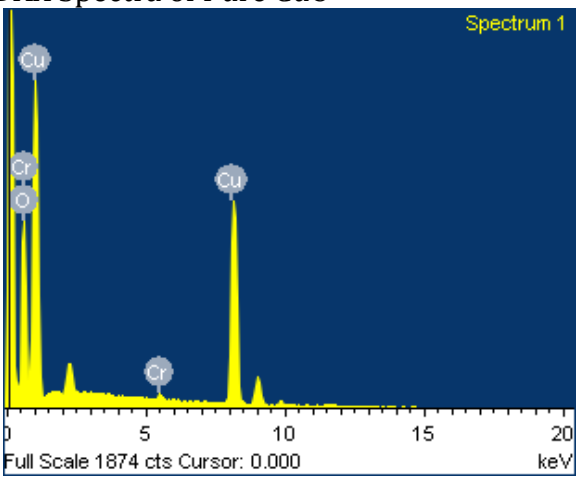


(b) SEM Micrograph and EDAX Spectra of 2 mol% Cr:CuO

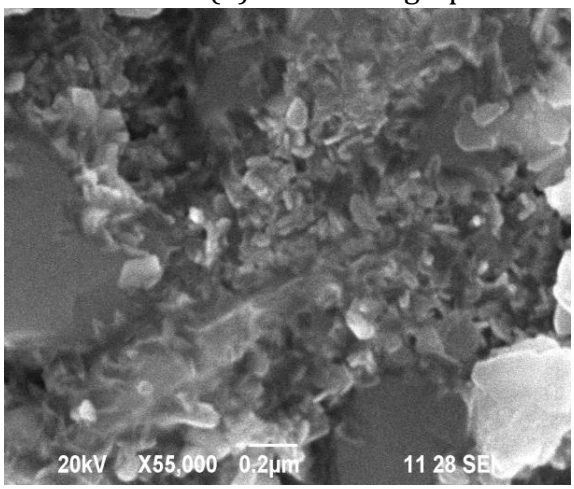


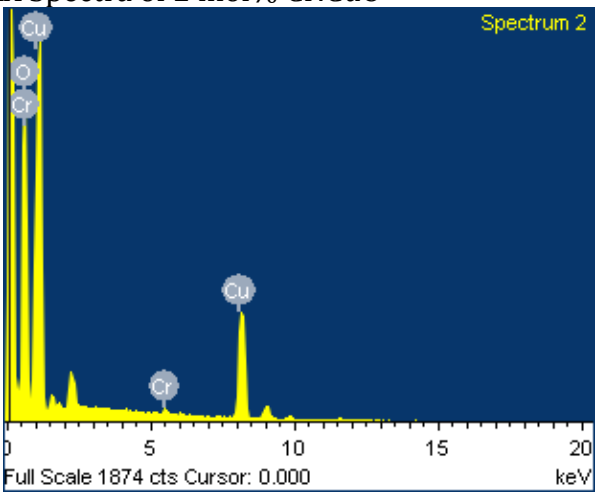


(c) SEM Micrograph and EDAX Spectra of 4 mol% Cr:CuO

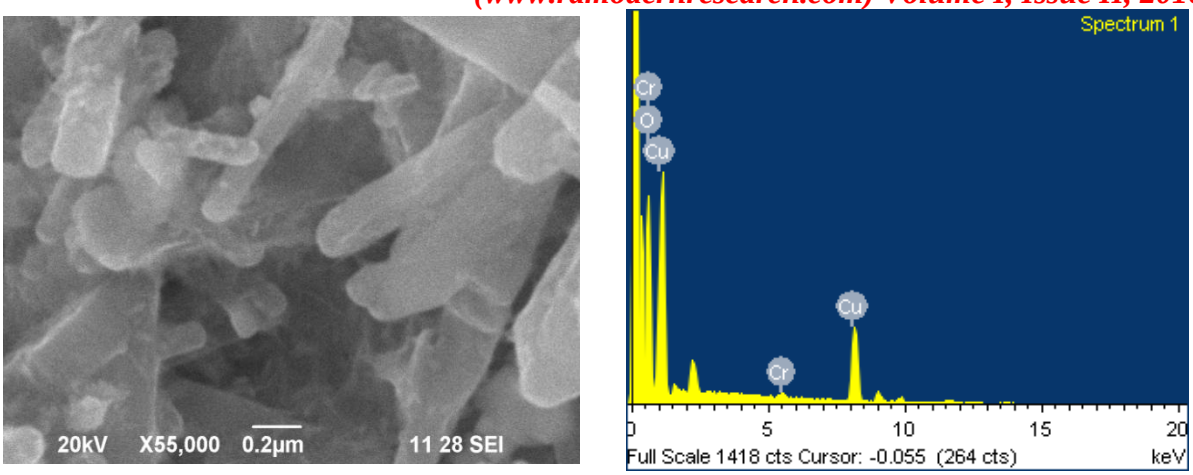


(d) SEM Micrograph and EDAX Spectra of 6 mol% Cr:CuO

Figure 3: SEM micrographs and EDAX spectra of CuO nanostructures

It can be concluded from the results of XRD and EDAX that the Cr is successfully substituted in all the doped samples. The variation in particle size matches well with the XRD results. However, the average particle size obtained from SEM analysis is slightly greater than the values calculated from XRD measurements. It may be due to the aggregation of particles at higher calcinated temperatures [18].

Table 2: EDAX Analysis

| Sample | Atomic Percentage (%) | | | Weight Percentage (%) | | |
|---|---|---|---|---|---|---|
| | Cu | O | Cr | Cu | O | Cr |
| CuO | 55.90 | 44.10 | - | 75.81 | 24.19 | - |
| CuO with 2 mol % of Cr | 37.78 | 61.60 | 0.62 | 70.22 | 28.83 | 0.95 |
| CuO with 4 mol % of Cr | 21.90 | 77.40 | 0.71 | 52.18 | 46.44 | 1.38 |
| CuO with 6 mol % of Cr | 25.02 | 74.13 | 0.85 | 56.38 | 42.05 | 1.57 |

**Optical Analysis:**

**Ultraviolet-Visible Spectroscopy (Uv-Vis):**

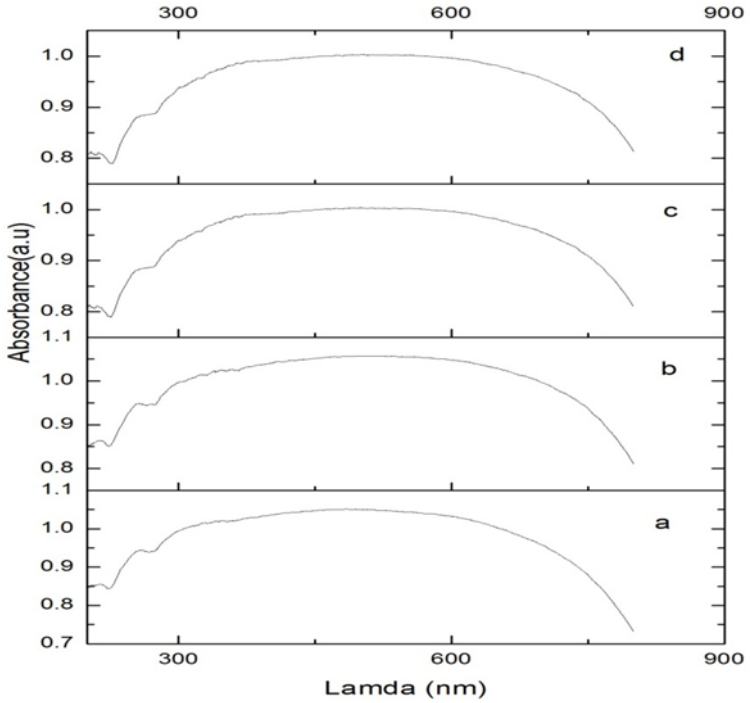


Figure 4: The Absorbance Spectra for (a) CuO and (b-d) Cr doped CuO (2, 4, 6 mol %)

For any nanoparticle system it is found that, the surface to volume ratio (i.e. aspect ratio) is higher than their bulk counterpart. More atoms/molecules are arranged

on the surface of nanoparticle due to which, the surface chemistry of these materials is of immense interest. For this purpose the UV–Vis spectral analysis was carried out between 200 nm and 900 nm for pure and Cr doped samples and depicted in Fig-4.Pure and Cr-doped CuO shows a broad absorption peak extending from UV to Visible region for all the samples [19]. This confirms the semiconducting nature of the CuO nanocrystals that can be widely used in applications related to photovoltaic and photocatalytic activities

The absorption data was used to generate Tauc plots to determine the energy gap of the pure and doped CuO which indicate a direct energy-gap for all the samples. The band gap energy ($E_g$) of the synthesized CuO and CuO with Cr (2, 4 and 6 mol%) were estimated by extrapolating the linear portion of $(\alpha h\nu)^2$ versus ($h\nu$) plots using the relation $\alpha h\upsilon = A(h\nu - E_g)^{1/2}$ Band-gap values found to be larger than the bulk CuO (1.2 eV), which can be attributed to the quantum confinement effect [20]. Further the values found to increase as the doping concentrations increased slightly from 2.1eV to 2.5eV in accordance with observations made in XRD plot.

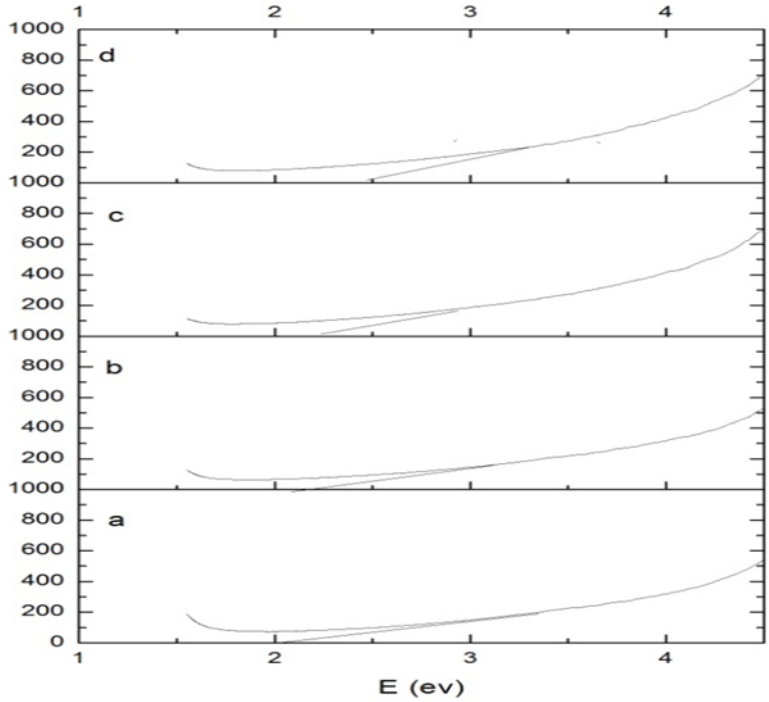


Figure 5: The Bandgap Energy for (a) CuO and (b-d) Cr doped CuO (2, 4, 6 mol %)

The PL property of the CuO nanoparticles is significantly influenced by the particle size, morphology and composition. The method of preparation has added influence on emission properties. Various research groups have done investigations on the Photoluminescence (PL) studies of CuO nanoparticles [21-26].The reported emission spectrum of CuO nanoparticles generally consists of many bands in the range 200–700 nm (visible region). Fig- 6 shows the PL spectra of pure and Cr doped CuO nanostructures prepared by co-precipitation method. The PL Spectrum shows UV as well as visible emissions and exhibit UV emission peak at 373 nm and visible emission peak in the violet region 447 nm, a small hump in blue regions 487 nm and green emission peak at 530 nm. The origin of UV emission in CuO is due to the recombination of electron–hole pair in free-excitons [21]. The luminescence blue bands at 447 nm are caused by transition vacancy of oxygen and interstitial oxygen [21,22] The PL peak at 550 nm corresponds to green emission, arises from the singly ionized oxygen vacancy[23,24] Comparing the pure and Cr doped PL spectra it is observed that doping

does not create any new emissions whereas there is a profound change the intensities of the prominent peaks. [26]

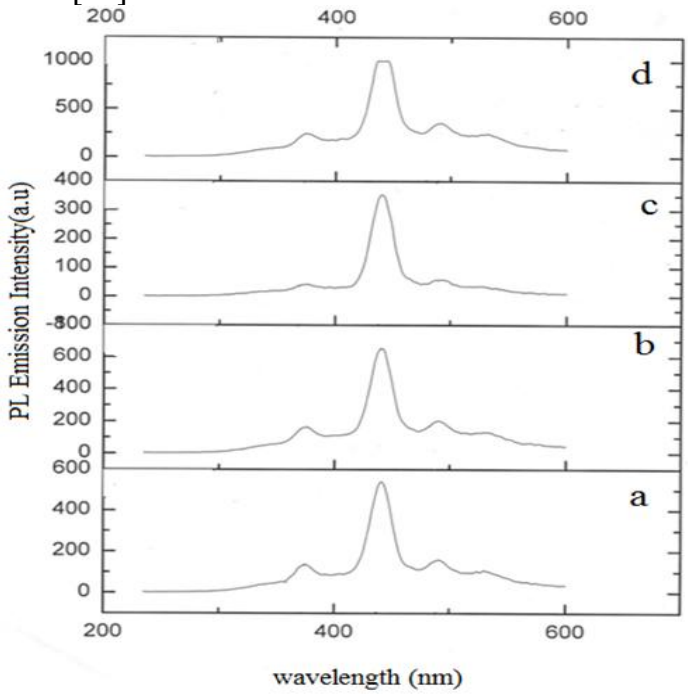


Figure 6: (a) The PL for CuO and (b-d) Cr doped CuO (2, 4, 6 mol %)

**Fourier Transform Infrared Spectral Analysis:**

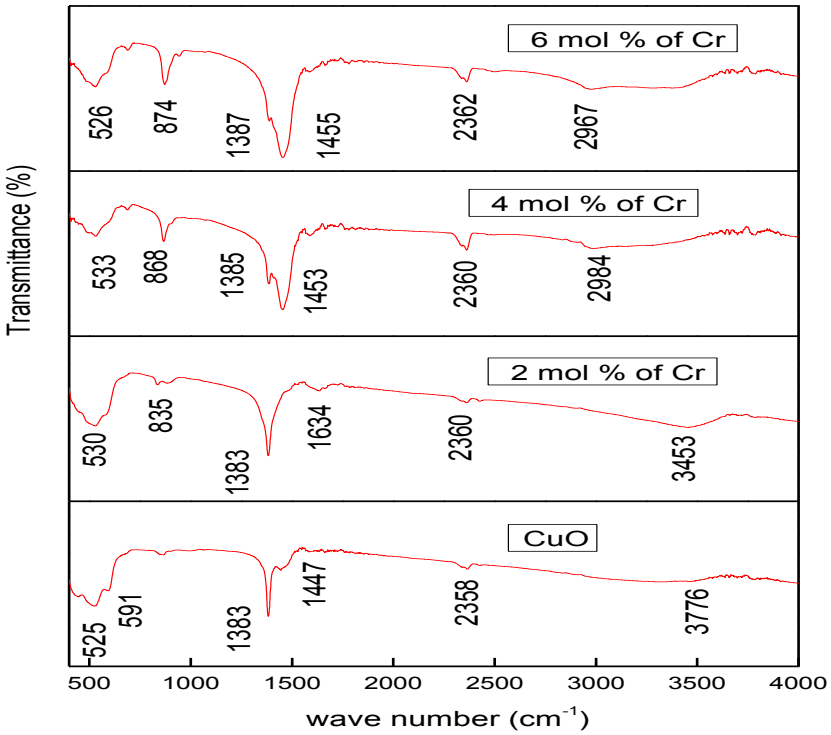


Figure 7: The FTIR for(a) CuO and (b-d) Cr doped CuO (2, 4, 6 mol %)

FTIR analysis can give qualitative (identification) analysis of materials as well as with suitable standards, can be used for quantitative (amount) analysis. FTIR spectra were recorded for all the prepared pure and Cr doped-CuO nano particles at room

temperature in frequency region 600 - 400 $cm^{-1}$ and the spectra is shown in Figure 7.The absorption peaks in the range of 1380-1640$cm^{-1}$ noted for all the samples may be assigned to alkyl(O-H) bending vibrations combined with copper atoms[27]. The absorption peaks at 2358 -2362 $cm^{-1}$ attribute to C=N stretching. The week band in the range of 2984 and 2967 $Cm^{-1}$ may be assigned to alkyl C-H stretching present [28]. The peaks at 525-584 $cm^{-1}$ are attributable to Cu-O stretching modes and the peaks at 591cm-1 and 691cm-1 are due to Cu-O stretching vibrations [29, 30]. The peak at 3432 $cm^{-1}$ is due to the vibration mode of the absorbed water [31]. The appearance of peaks around 850 $cm^{-1}$ confirms the presence of Cr in the doped samples. [32]

**Measurement of Solar Parameters:**

In order to investigate the performance of the pure and Cr doped CuO nanostructures as light absorbing solar materials, heterojunctions ITO/$TiO_2$/CuO:Cr/ Cu (Cr= 2%, 4% and 6 mol %) were fabricated as discussed earlier. The current-voltage characteristics and the Power-Voltage characteristics were drawn for all the samples and depicted in Figs. 8 and 9. It is observed that the noisy appearance in both V-I and P-V plot of the pure CuO has been completely rectified in the doped samples. It's also observed the increase in the $P_{max}$ leads to the increase in the efficiency "ŋ" of the solar cell. The solar cell parameters such as open circuit voltage (Voc), short circuit current (Isc), power maximum (Pmax) and fill factor (FF) are summarized in Table 3.

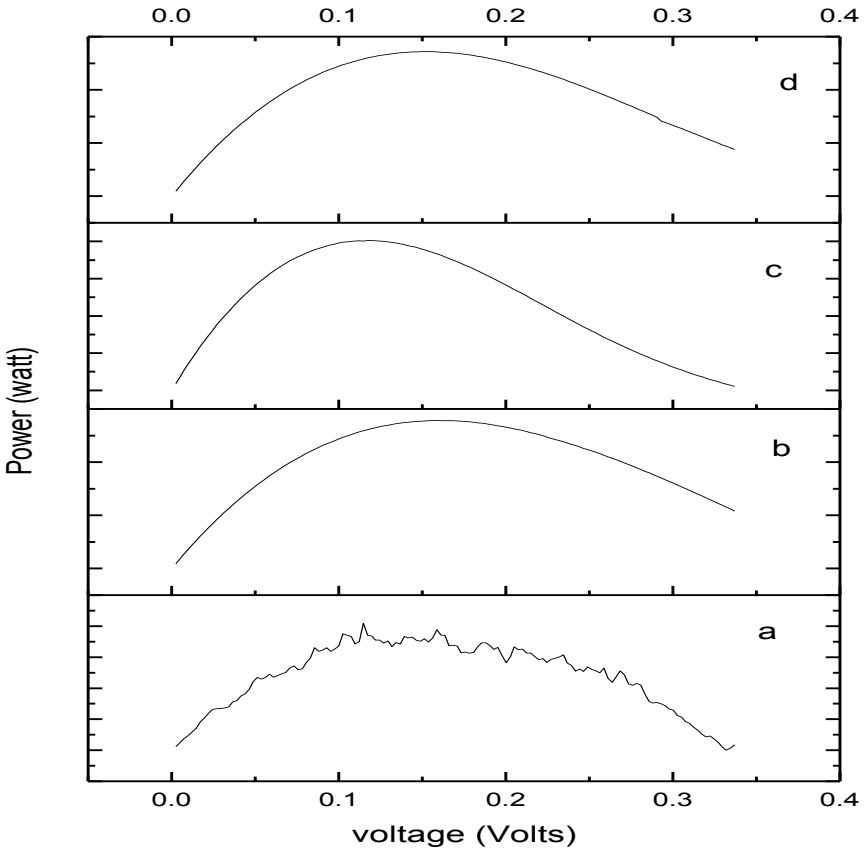


Figure 8: The P-I graph for(a) CuO and (b-d) Cr doped CuO (2, 4, 6 mol %)

The poor value for efficiency "ŋ" may be due to the shunt resistance created by the polycrystalline nanopowder-thin film that arises from the grains which may lead to the leakage through the boundries. The curvature observed near Voc is due to insufficient/non ohmic contact [33]. Ideally, the shunt resistance should be infinite so

that there is no leakage. This will be observed when the photocurrent -photovoltage plot is perfectly rectangular as in the ideal case. The low shunt resistance may be caused by the leakage of current across the semiconductor surface. The presence and orientation of the crystallite boundaries may be responsible for current leakage.

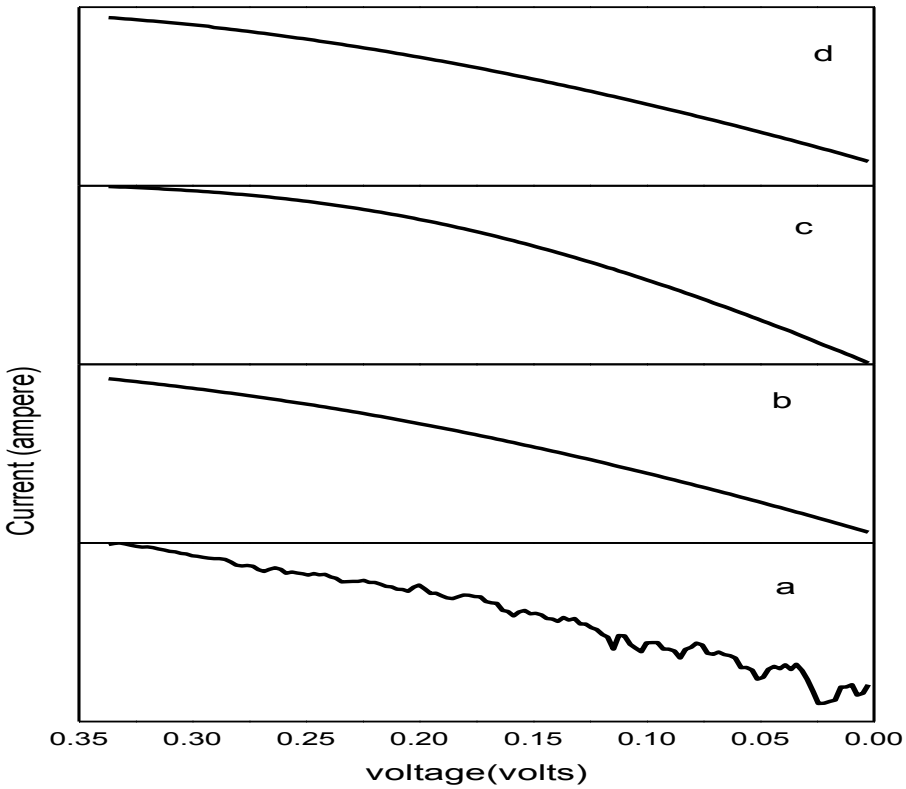


Figure 9: The V-I graph for (a)CuO and (b-d) Cr doped CuO (2, 4, 6 mol %)

Table 3: Solar Cell Parameters

| Sample | Open circuit Voltage V | Short circuit Current µA | Fill Factor | Area sq cm | Efficiency % |
|---|---|---|---|---|---|
| CuO | 0'4907 | 2.3825 | 0.17512 | 1.6 | 0.016619 |
| CuO +2% | 0.4907 | 3.7588 | 0.15086 | 1.6 | 0.022586 |
| CuO+4% | 0 4907 | 1.489 | 0.110078 | 1.6 | 0.06531 |
| CuO +6% | 0 4907 | 7'7697 | 0.14257 | 1.6 | 0.04412 |

**Conclusions:**

Pure and Chromium doped CuO nanostructures were synthesised by Co – precipitation method and was subjected to structural, morphological elemental and optical analysis. The XRD studies reveals the reduction in the grain size due the doping of Cr and its substitutional nature in the crystal lattice without altering the monoclinic structure of the host material.SEM analysis confirms the change in the morphology created by the dopant concentrations of Cr ions. EDAX analysis confirms the presence of the dopant ion in the host material. From the absorption spectra, the band gap values were calculated and found to be increasing from 2 eV to 2.5 eV in accordance with the XRD results.PL spectra show profound changes in the intensities of the emissions without any new emissions due to doping of Chromium ions. Heterojunctions of pure and Cr doped CuO nanostructures were indigenously made by Doctor-Blade method and cell parameters were measured using a solar simulator. The observations made revealed that the doping has created some changes in the cell parameters current

density Jsc, FillFactor (FF) and solar cell efficiency "ŋ" and the value of "ŋ" around 0.04% . The poor value may be due to the shunt value created by the polycrystalline powder –thin film that arises from the grains which may lead to leakage path through the boundaries.

**References:**

1. Guijarr N Lutz , T Lana -Villarreal T O'Mahony F Gó mez,R. Haque S. A J. Phys. Chem. Lett. 2012 3 1351–1356
2. Jia Huang, Zhigang Yin and Qingdong Zheng, Energy Environ. Sci., 2011 4 3861-3877.
3. ] Jose, R.; Thavasi, V.; Ramakrishna, S. J. Am. Ceram. Soc. 2009, 92, 289–301
4. Anta, J. A.; Guillén, E.; Tena-Zaera, R. J. Phys. Chem. C 2012, 116, 11413–11425.
5. M. Dahrul, Husin Alatas , Irzaman Procedia Environmental Sciences , 2016 33 661.
6. R. Ranjbar-Karimi, Bazmandegan-Shamili, A., Aslani, A., and Kaviani, K., Physica B: Condensed Matter, 2010 405 15 3096.
7. Yusheng Xia, Xuxin Pu, Jie Liu, Jie Liang, Pujun Liu, Xiaoqing Li and Xibin Yu, J. Mater. Chem. A, 2014 2 6796-6800
8. Peng Wang, Xinhong Zhao, and Baojun Li 2011 19(12), Optics Express 11271
9. L. Obulapathi, A. Gurusampath Kumar, T. Sofi Sarmash & T. Subba Rao, International Journal of Nanotechnology and Application (IJNA) 4(4) 2014 29-34.
10. S. Bhuvaneshwari, N. Gopalakrishnan Journal of Alloys and Compounds 654 (2016) 202e208
11. P Gwizdz Merta Redecka Katarzyna Zakrzewske Procedia Engineering 87:1059-1062 · December 2014
12. Prashant V. Kamat, J. Phys. Chem. C (2008)112 18737–18753.
13. N.Gomesh1, A.H.Ibrahim1, R.Syafinar1, M.Irwanto1, M.R.Mamat1, Y.M Irwan1,
14. U.Hashim2, N.Mariun3 International Journal Series in Engineering Science (IJSES), 1(1) 2015 49-56.
15. J. M. Wesselinowa, Physics Letters A 375 (2011) 1417-1420] Alan MENG
16. Sajjad Mohebbi Somayeh Moaei Amir Reza Judy Azar Journal of Applied Chemistry 2013 8 27
17. Jing Xing Zhenjiang Li Q ingding ACS Applied Materials and Interfaces
18. Mou Pal Umapada Pal Justo Migual Gracia Y Jimenez and Felie Perez Rodriguez NanoScale Res. Let 2012 7(1)
19. V. Ponnarasan A. Krishnan Adv Studies Theor Phys 2014 8 (6) 251-258
20. C. C. Vidyasagar, Y. Arthoba Naik, T.G. Venkatesh, R. Viswanatha Powder Technology 214 (2011) 337–343
21. S. G. Rejith C Krishnan Advances in Applied Research area 2013 4 (2) 103-104
22. M. Nillohit, S. Bibhutibhushan, K. M. Swarup, M. Utpal, K.B. Sanjib, C. M. Bibhas, G. K. Gobinda, M. Anup, , J. Mater. Lett. 65 (2011) 3248–3250.
23. C. Prakash, G. Anurag, K. Ashavani, J. Superlattices Microstruct (2314), http:// dx.doi.org /10.1016/j.spmi.2013.04.026 (
24. Hafsa Siddiqui, M.S. Qureshi, Fozia Z. Haque 125(17) September 2014 4663.
25. P. Chand, A. Gaur, A. Kumar, Superlattices Microstruct, (2013) 60 129.
26. S. S. Changa, H. J. Leea, H. J. Park, Ceram. Int, (2005) 31 411.
27. Kankanit Phiwdang, Sineenart Suphankij, Wanichaya Mekprasart and Wisanu Pecharapa, Energy Procedia 34 (2013) 740-745.
28. Rohit Guin, Shakila Banu A, Gino A Kurian, International Journal of Pharmacy and Pharmaceutical Sciences, ISSN- 0975-1491 (2015) 7.

29. Kankanit Phiwdang, Sineenart Suphankija, Wanichaya Mekprasarta,b and Wisanu Pecharapaa, Energy Procedia 34 ( 2013 ) 740.
30. Anitha Sagaadevan Ethiraj,,Dae Joon Kang,nanoscale research letters7(1) 70 (2012).
31. Ahmad Rahnama, Mehrnaz Gharagozlou, Springer Science + Business Media LLC (2012) 44 313-322.
32. Mihali Mihaylob Anna Penkova Konstantan Haglivenow, Journal of Molecular Analysis A:Chemical 426 Part A.
33. K. L. Chopra, S. R. Das, Thin Film Solar Cells: Plenum Press-New York 1983 159.